



ARTICLE

A Computational Study on the Effect of Bifurcation Lesions with Different Structures on Blood Velocity and Temperature

Haoyu Wan, Heng Zhang and Zhizhu He*

Vehicle Engineering, College of Engineering, China Agricultural University, Beijing, 100083, China

*Corresponding Author: Zhizhu He. Email: zzhe@cau.edu.cn

Received: 15 July 2020 Accepted: 07 February 2021

ABSTRACT

Treating coronary bifurcation stenosis is still a challenging task. Existing procedures still display a relatively small rate of success. This paper aims to investigate numerically the effect of bifurcation lesions with different structures on the dynamics of blood flow and related temperature. The problem geometry is parametrically varied by changing the bifurcation angle and radius. A finite volume method is used to simulate the three-dimensional flow. The effects induced by the structure of the stenosis, the artery bifurcation angle and radius, and the inlet velocity of blood are discussed in terms of flow pattern, pressure distribution, and shear stress at the blood wall. The heat transfer from the solid tissue is also determined for different stenosis configurations. The present study has been conducted with the explicit intention to generate useful data for the development of methods curing the vascular stenosis with thermal ablation.

KEYWORDS

Bioheat transfer; arterial bifurcation; stenosis; blood thermal effect

1 Introduction

Cardiovascular disease induced by bifurcation lesions is one of leading causes of death in humans, which remains a significant challenge for its treatment due to a higher risk of restenosis [1]. Many lesions located on the blood vessel were induced by the combined effect of hemodynamics and physiologic process, which often affects the plaque and stenosis formation, such as a chronic disease of atherosclerosis [2]. The domains near branch points and the outer wall of bifurcation with low shear stress are often lesions appearances, such as aneurysms [3] and stenosis [4,5]. The local hemodynamic forces play a fundamental role in the lesion formation [6], which impacts the localization and progression of particle sedimentation and plaque formation [7]. The blood computational fluid dynamics is an essential tool to be used for investigating the formation mechanism of the plaque, which would be a benefit for better clinical outcomes [8,9].

In the past, there has been a variety of studies to investigate the impact of blood vessel bifurcation on blood fluid dynamics [10] and heat transfer. Chiastra et al. [11] have applied the computational fluid dynamics method to study the influence of the bifurcation angle on the coronary fractional flow, which indicates that the side-branch pressure drop becomes high for a larger bifurcation angle. Cutri et al. [12] have studied the drug delivery mechanism for different stenting techniques in coronary bifurcations



through fluid dynamics simulation. Otero-Cacho et al. [13] have investigated the determination of hemodynamic risk for vascular disease in planar artery bifurcations through numerical simulation method and the experiments based on the microchannel. The results indicated that the low-velocity regions and low shear stress zones are located near bifurcations' outer walls. The work from Hossain et al. [14] have focused on the external magnetic field's impacts on the interaction between the flexible membrane wall and flowing nanofluid in a collapsible arterial network, where the stenosis structure was considered. Santabrata Chakravarty et al. [15] have investigated the dynamic response of heat and mass transfer to blood streaming through the arteries under stenotic conditions, while they have not considered the vessel bifurcation. Wang et al. [16] have found that fractal vascular trees have an important effect on tissue temperature and intracellular ice formation during the combined cryosurgery and hyperthermia for cancer therapy. In addition, Zheng et al. [17] have studied the thermal effects of bifurcation on the iceball morphology during cryosurgery. Recently, Zhang et al. [18] investigated the impact of a bifurcation structure on the heat transfer and temperature distribution of pulsatile blood flow.

The bifurcated artery with stenosis has a complicated structure, which would lead to more complex blood flow distribution, and induce the heterogeneous heat transfer surrounding bifurcation stenosis. As is well known, less investigation contributes to the effects of bifurcation stenosis on both the temperature response and blood flow pattern. In the present study, a parametric geometry model is introduced to construct a close-to-real arterial bifurcation with different bifurcation angle and radius. The three-dimensional flow dynamics and heat transfer simulation model is developed through the finite volume method. The discussion was then made on the effects of stenosis structure, artery bifurcation and the inlet velocity of the root artery on the blood flow pattern, pressure distribution and shear stress at the blood wall, respectively. In addition, the heat transfer from the solid tissue was also investigated for different stenosis structure.

2 Geometry and Mathematical Model

2.1 Geometric Model

The arterial bifurcation of the blood vessel, including the main vessel and two branch vessels, is determined by a parametric geometric model [19], which could characterize realistic configuration of arterial bifurcation. The different arterial bifurcation structures are given in Fig. 1.

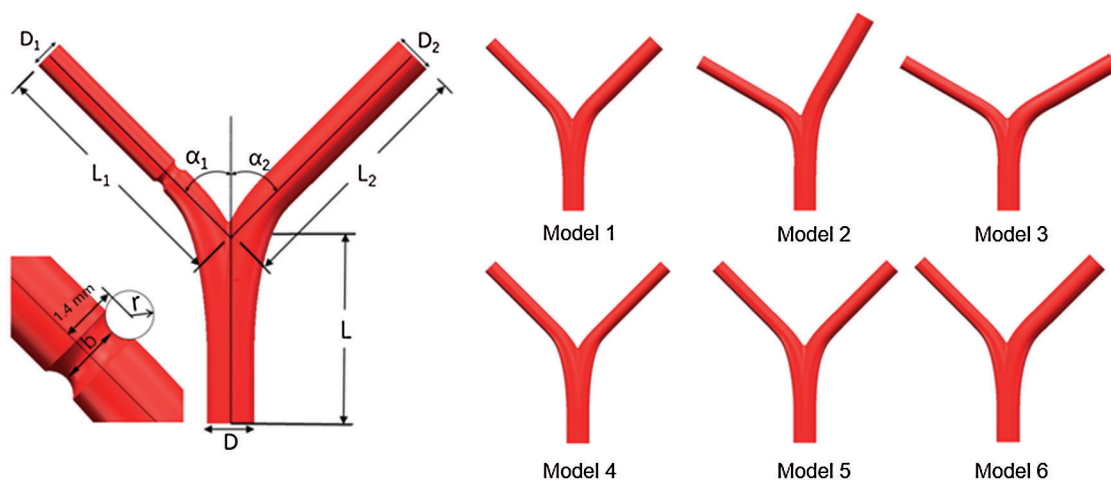


Figure 1: Schematic of the bifurcated artery and computational field

The main vessel is considered with diameter $D = 3.30$ mm and length $L = 13$ mm, the left branch (LB) vessel length has $L1 = 18$ mm and right branch vessel diameter with length $L2 = 18$ mm, respectively. In addition, two branches of angles are set as α_1 and α_2 , respectively. The lesion is cut with a circular scan of radius r [20]. The minimum diameter of the stenosis is noted by b , and the radius r is 0, 0.6 mm, 0.8 mm, and 1.0 mm, respectively. Thus, the minimum diameter b corresponds to 2.1 mm, 1.6 mm, 1.2 mm, and 0.8 mm, respectively. Six different models are created by changing the parameters, and each model corresponds to four other lesions, as shown in [Tab. 1](#).

Table 1: Parameter example (unit: mm)

Model	Case	D_1	D_2	α_1	α_2	r	b
1	1	2.10	2.77	45°	45°	0.0	D_1
	2					0.6	1.6
	3					0.8	1.2
	4					1.0	0.8
2	5	2.10	2.77	30°	60°	0.0	D_1
	6					0.6	1.6
	7					0.8	1.2
	8					1.0	0.8
3	9	2.10	2.77	60°	60°	0.0	D_1
	10					0.6	1.6
	11					0.8	1.2
	12					1.0	0.8
4	13	2.10	2.00	45°	45°	0.0	D_1
	14					0.6	1.6
	15					0.8	1.2
	16					1.0	0.8
5	17	2.10	2.40	45°	45°	0.0	D_1
	18					0.6	1.6
	19					0.8	1.2
	20					1.0	0.8
6	21	2.10	3.10	45°	45°	0.0	D_1
	22					0.6	1.6
	23					0.8	1.2
	24					1.0	0.8

2.2 Fluid Dynamics Simulation Method

In this paper, the commercial software of ANSYS-FLUENT was used to model the mass conservation, momentum conservation, and energy conservation equations of blood, described by

$$\begin{cases} \nabla \cdot V = 0 \\ \rho V \nabla V - \mu \nabla^2 V = 0 \\ \rho c V \nabla T - k \nabla^2 T = 0 \end{cases} \quad (1)$$

where ρ denotes the blood density, μ for its viscosity and k for the thermal conductivity. The blood is considered an incompressible viscous Newtonian fluid. The non-slip boundary condition is assumed at the blood wall, the aortic blood inlet flow rate is set as 0.2 m/s [20], and the outlet condition is given by mass outflow. For the temperature field, the inlet temperature is assumed as the constant as needed.

The unstructured mesh through ANSYS-ICEM is considered here, where the geometry models were established from software of Solidworks. The fluid dynamics of blood is set as a laminar type. The density of blood is set to 1050 kg/m³, and the viscosity of blood is 0.0035 Pa·s. The time-independent blood flow field is solved through using the SIMPLE algorithm, and the stable temperature field through the second-order upwind algorithm is obtained [17]. The mesh quality significantly affects the simulation results, while the excessively small mesh size would lead to high computing resources needed. All the test cases are carried out with the same computer configuration (CPU: E5-2650@2.3 GHz; Memory size: 64 GB). In order to verify the accuracy of CFD model, the comparison of the experiment results of Gijssen et al. [21] at $Re = 270$ with that from our simulation method is conducted, which indicates that our CFD model is accurately consistent with the experiment results as presented in Fig. 2. In order to further ensure the calculation accuracy and computational speed, local encryption is considered to meet the calculation accuracy of the lesion and the bifurcation, as shown in Fig. 3.

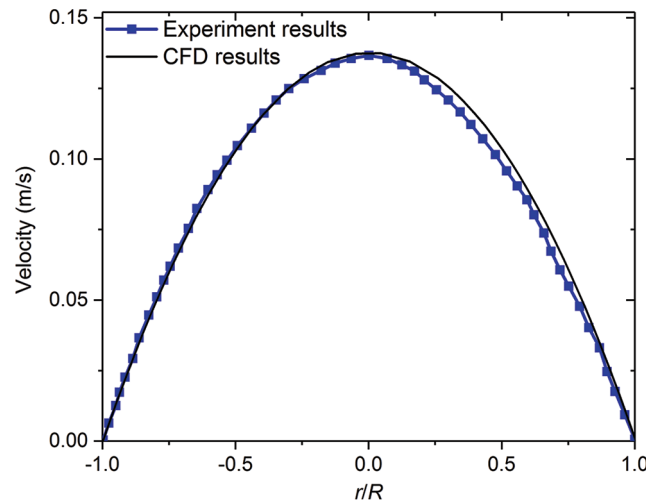


Figure 2: Comparing axial velocity on a line segment at a root vessel ($D = 8$ mm) with experimental results of Gijssen et al. [21]

The grid independence results are shown in Tab. 2, which has indicated that the total number of meshes for each model is between 8×10^5 and 12×10^5 , obtaining accurate numerical results (relative errors of blood velocity is smaller than 2%).

The flow ratio is calculated by the following formula [22,23]:

$$\frac{Q_1}{Q_2} = \left(\frac{D_1}{D_2} \right)^{2.27} \quad (2)$$

where Q_1 and Q_2 are the flow rates of the diseased bifurcation vessel and the main bifurcation vessels, respectively. For Model 1-3, the calculated flow distribution ratio is set as 35%: 65%. In order to further study the flow rate effects, other two flow ratios 30%: 70% and 40%: 60% are taken into accounts. The calculated flow rates for Models 4, 5 and 6 are set as 53%: 47%, 42.5%: 57.5% and 29%: 71%, respectively.

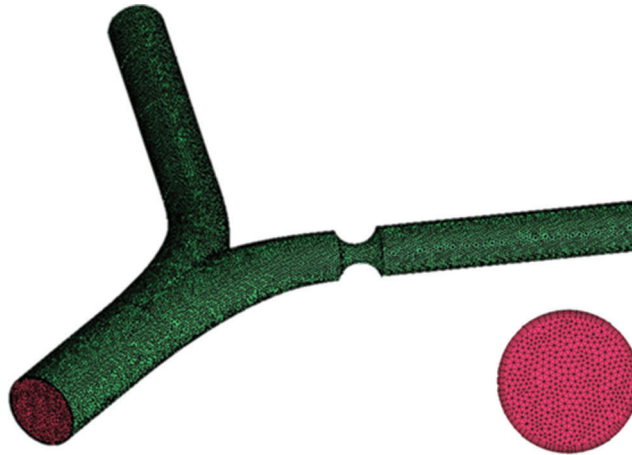


Figure 3: Grid and boundary layer diagram

Table 2: The grid independence results

Grid number	2×10^5	4×10^5	6×10^5	8×10^5	12×10^5
Outlet velocity(m/s)	0.295	0.313	0.346	0.348	0.348

3 Results and Discussion

Fig. 4 shows the flow field contours of Model 1 at different flow ratios with varying sizes of stenosis. The blood has a high flow velocity at the center of the blood vessel. The blood velocity distribution of the two-branched vessels was mainly determined by the flow ratios and the vessel radius for the normal blood vessels. It is also noteworthy that the low blood velocity domains were found near the bifurcation wall [11]. When the stenosis occurs at the left branch (LB) vessel, the blood velocity at the lesion is significantly increased. When the stenosis degree increases, the blood flow velocity in the same section is more uneven, which may lead to the deposition of impurities on the wall surface and aggravate the disease.

As the minimum diameter b decreases, the maximum flow velocity of the blood increases. Taking Model 1 as an example, with a flow ratio of 35%:65%, the maximum flow rate of non-lesion blood is 0.36 m/s. However, when b is 0.8 mm, the maximum flow rate of blood reaches 1.46 m/s, which occurs at the lesion. Tab. 3 shows the blood flow rate at the center of the lesion. At the same flow ratio, the change in the bifurcation angle has less effect on the flow rate of the point. Model 2 (60o–30o) has a lower blood flow velocity at the central point of the lesion compared to Model 1 (45o–45o). The flow rate of Model 3 (60o–60o) is the largest among them.

The pressure drops $\Delta p_1 = p_0 - p_1$ is considered the difference between inlet pressure p_0 and LB outlet pressure p_1 , while the pressure drops $\Delta p_2 = p_0 - p_2$ set as the difference between inlet pressure p_0 and RB outlet pressure p_2 . Figs. 5a–5c) shows the pressure drop of Models-1~3 at three flow rates, respectively. Fig. 5d shows the pressure drop in different RB diameters of D2. The pressure drop Δp_2 is independent of the stenosis diameter b , and the change of minimum b hardly affects the pressure drop at the LB outlet. However, the pressure drops Δp_1 increases as b decreases. As shown in Fig. 4a, Model-1 with the

flow ratio is 35%:65%, the pressure drop Δp_1 reaches 0.88 mmHg for $b=2.1$ mm. When $b=0.8$ mm, the pressure difference between the two ends reaches 6.76 mmHg. As the diameter b decreases, the rate of pressure drop rise increases. As shown in Fig. 5b for Model-2 under the flow ratio of 35%:65%, the pressure drop Δp_1 increases by 0.64 mmHg in the process of the diameter b decreasing from 1.6 mm to 1.2 mm; and Δp_1 increases by 5.42 mmHg in the process of b reducing from 1.2 mm to 0.8 mm.

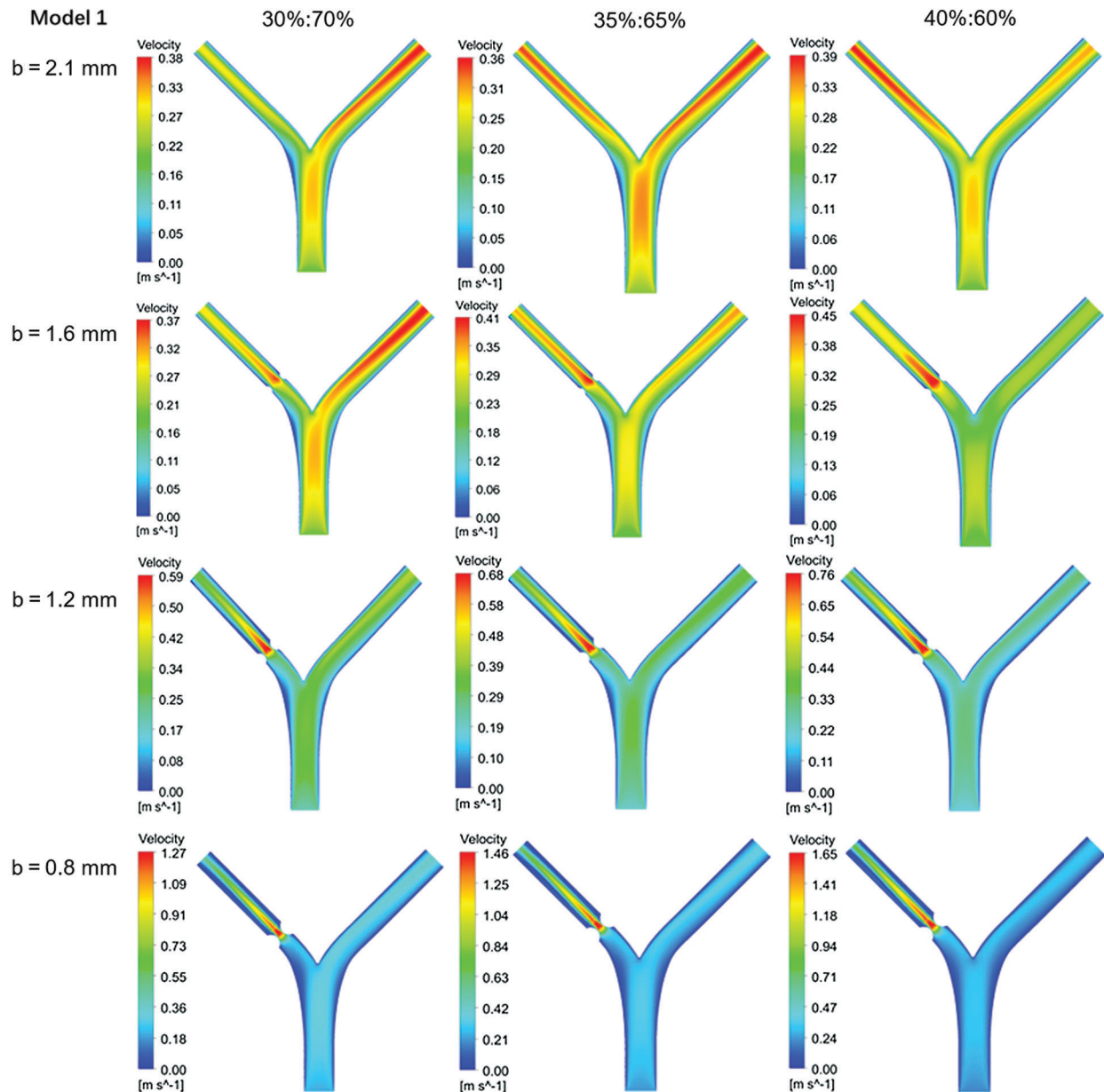


Figure 4: Flow rate contours of Model 1 with different flow distribution

Table 3: Blood flow rate at the center of the lesion

Case		Velocity/m·s ⁻¹			
		b = 2.1 mm	b = 1.6 mm	b = 1.2 mm	b = 0.8 mm
Model 1	30%: 70%	0.235	0.327	0.560	1.228
	35%: 65%	0.270	0.375	0.654	1.452
	40%: 60%	0.305	0.438	0.736	1.633
Model 2	30%: 70%	0.226	0.307	0.519	1.160
	35%: 65%	0.256	0.371	0.645	1.434
	40%: 60%	0.301	0.424	0.728	1.616
Model 3	30%: 70%	0.241	0.335	0.578	1.277
	35%: 65%	0.289	0.394	0.667	1.466
	40%: 60%	0.303	0.443	0.743	1.652

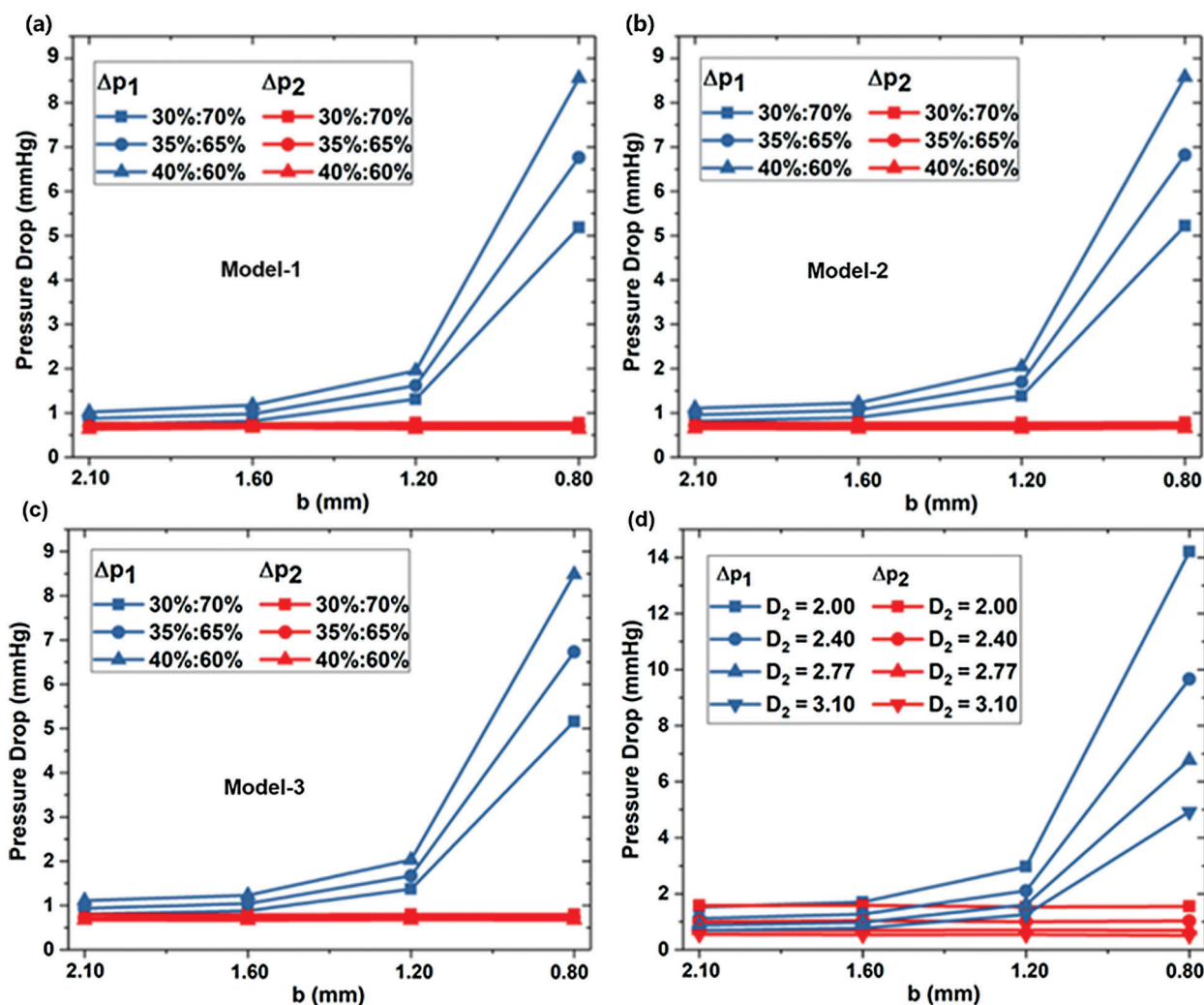


Figure 5: The dependence of pressure drops on stenosis sizes in different models (a) Model-1, (b) Model-2 and (c) Model-3, and for different D_2

Fig. 6 shows the relative intravascular pressure distribution of Models 1–3 at different b under a standard flow ratio of 35%:65%. Because of the diameter b reducing, the inlet pressure at lesion is higher. The outlet pressure at the lesion is lower so that the pressure at the near wall of the bifurcation is higher than that in the vicinity. It would increase with decreasing diameter b .

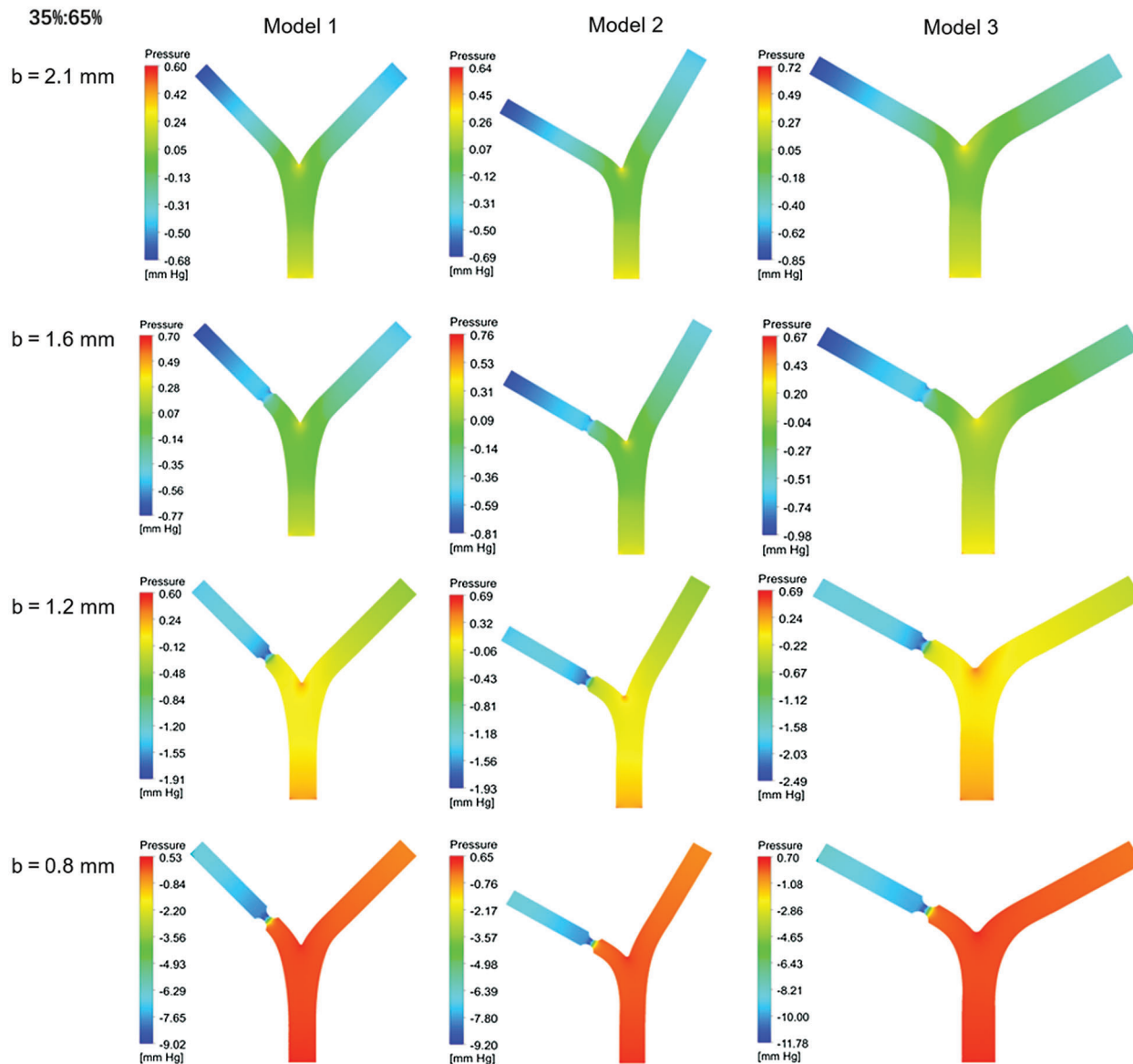


Figure 6: Pressure distribution for different blood flow ratio

Fig. 7 shows the wall shear stress (WSS) located at the bifurcation and the stenosis of the Model-1~3 under three kinds of flow rates. WSS at the bifurcation is small and does not change significantly with stenosis diameter b or bifurcation angle α_1 , α_2 . The maximum WSS at the bifurcation is 6.42 Pa. There was no significant difference in WSS among Models 1–3 under the same conditions. When diameter $b = 0.8$ mm and flow rate accounts for 30%, 35%, and 40%, the WSS at the diseased region is close to 80 Pa, 100 Pa, and 120 Pa, respectively. The WSS at stenosis of Model 2 and Model 3 is more

significant than Model 1, while the WSS difference between Models 2 and 3 is small. In consequence, increasing angle α_1 of LB will increase the wall shear stress.

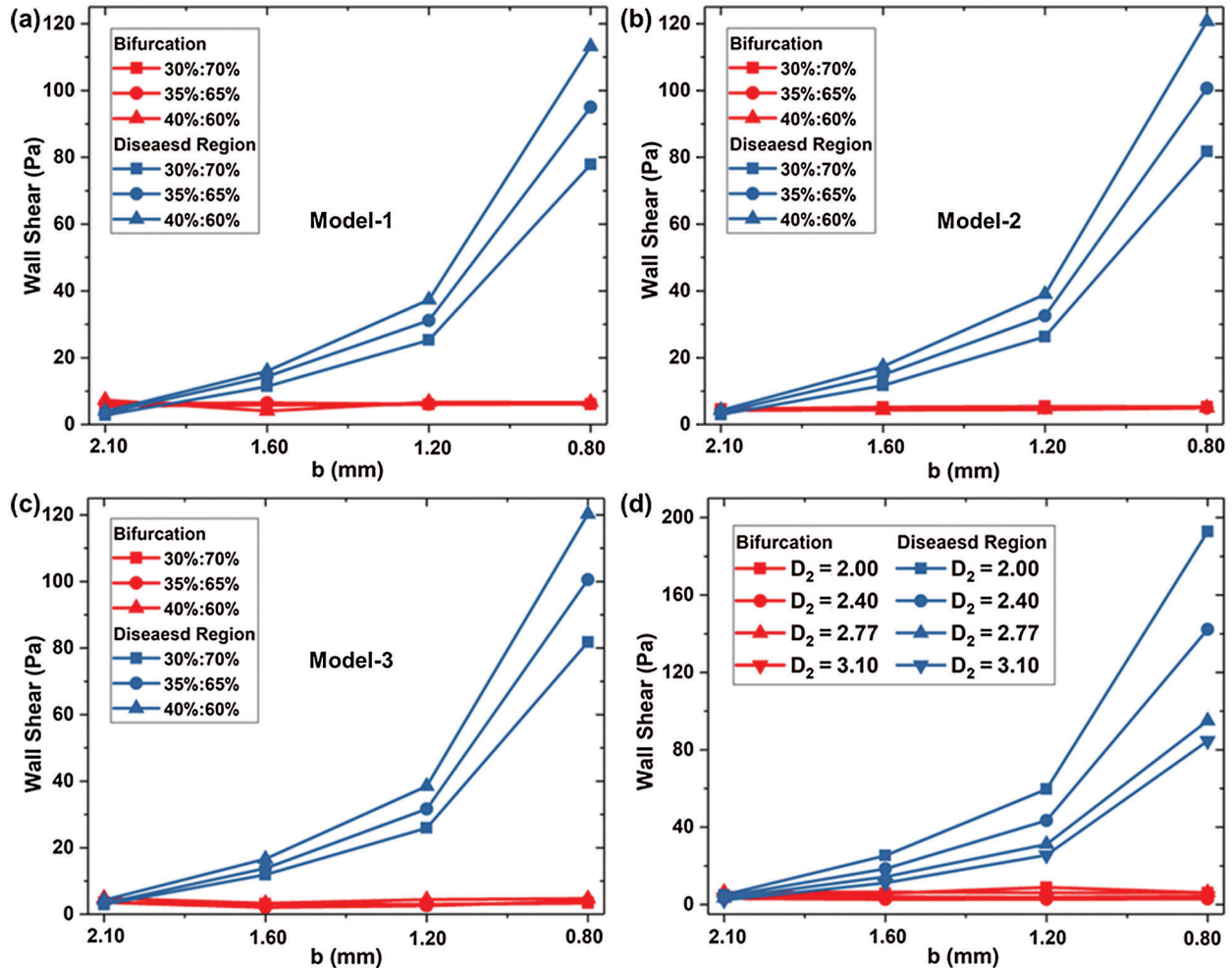


Figure 7: WSS located at the bifurcation and the stenosis for (a) Model-1, (b) WSS-2 and (c) Model-3; and the impact of D_2 on WSS (d)

Fig. 7d shows the WSS in different D_2 (Model 1, and Models 4–6) at bifurcation and lesion region. The WSS of the four models at the bifurcation almost keeps the same. The WSS of the lesion increases with the decrease of diameter b , and the smaller the diameter b , the faster WSS increases. At a standard flow ratio of 35%: 65%, when $b = 1.2$ mm, the WSS of Model 1 is 31.17 Pa, which has a rise of 16.79 Pa compared with $b = 1.6$ mm. When the minimum diameter of $b = 0.8$ mm, WSS increases by 68.36Pa compared to 1.2 mm. D_2 variation has a significant impact on the WSS at the stenosis with the small diameter of b . For $b = 0.8$ mm, the WSS at stenosis is increased by 10.4Pa with D_2 reducing from 3.10 mm to 2.77 mm.

Fig. 8 shows the contour of WSS in different D_2 (Model 1, and Models 4–6) at standard flow rates. The WSS patterns have similar distribution for other models. However, WSS changes obviously at stenosis as the minimum diameter b decreases.

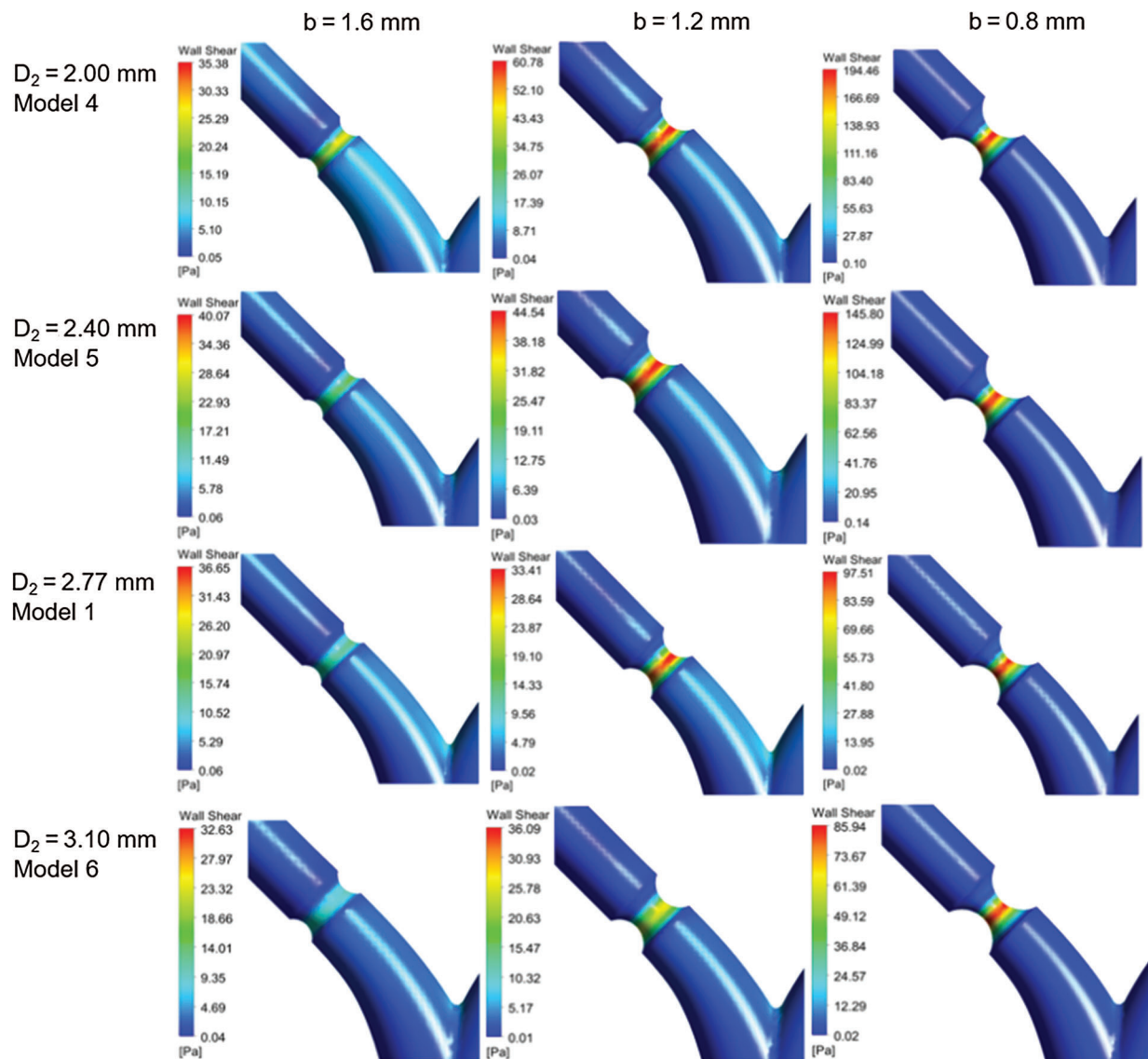


Figure 8: Contour of WSS for different models

Based on the simulation results of the flow field, a series of heat flux is set at the vessel wall to study the blood temperature distribution due to the solid tissue impact. The initial blood temperature assumes as 37°C . The thermal conductivity of blood is set to $0.55 \text{ W/m}\cdot\text{K}$ [17]. Fig. 8 shows the steady temperature field of Model-1 ($b = 2.1 \text{ mm}$ and $b = 1.2 \text{ mm}$), where the heat flux is set as 5000 W/m^2 . The temperatures distribution located at sections denoted by A, B, C and D as shown in Fig. 9a are given. When the heat transfer between the vessel and solid tissue is considered, the blood temperature at the inlet is set as 37°C . As the blood flows, the temperature near the wall rises, and the temperature on both sides is higher than that on the inside. This is related to the difference in flow velocity. The inner side of the blood still maintains a higher flow velocity, while the outer side has a larger temperature gradient. The average temperature of the blood near the top of the branching vessel is lower than that below.

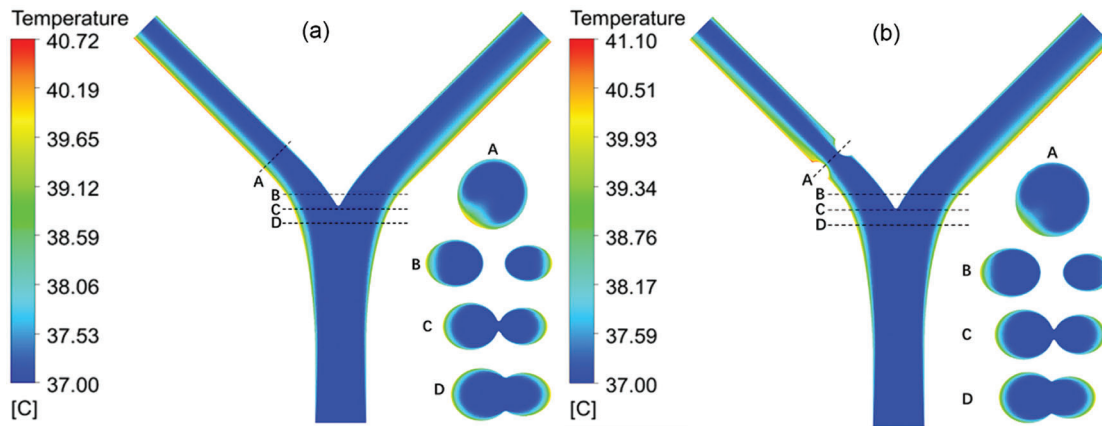


Figure 9: The temperature contour of the blood vessel for (a) $b = 2.1$ mm and (b) $b = 1.2$ mm

The cross-section temperature contour shows that at the bifurcation, the temperature near the center barely changed, while the temperature around the two sides changed significantly. Due to the decrease of diameter, the flow concentrates and the flow rate increases accordingly. The change of temperature at the lesion is small. In addition, as the diameter returns to normal and the flow velocity is low at a position below the outlet of the lesion, the max temperature occurs at this position. In different lesion diameter b , the temperature rises linearly with the heating power. In the absence of lesions ($b = 2.1$ mm), both the max temperature and the outlet temperature are minimal. This is because the flow is relatively stable, and there is no slow-speed area like lesion happens. The LB outlet center temperature is shown in Fig. 9. When a lesion occurs, with the decrease of b , the max temperature decreases and the outlet temperature increases.

On the one hand, the decrease of b increases the flow velocity. It makes the flow at the outlet more uneven (see Fig. 10). When $b = 1.6$ mm, the max temperature is the highest due to its low flow rate area below the lesion. However, the high-velocity area of flow after the lesion is larger than other conditions, so the outlet temperature is smaller. When $b = 0.8$ mm, the maximum velocity increases so that the max temperature is small. Nevertheless, the area with a high flow rate is small and the blood velocity around it is low, so that heat is transferred to the blood vessels and the outlet temperature increased significantly. Besides, the smaller the lesion diameter b is, the less obvious the decrease of vascular max temperature is, and the more obvious the increase of outlet temperature.

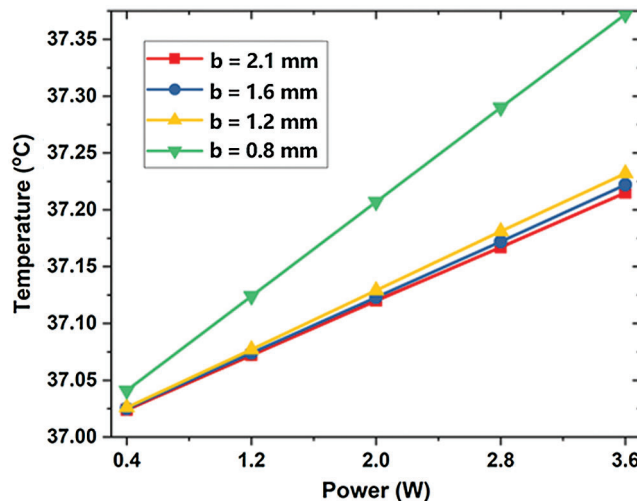


Figure 10: The maximum temperature of LB outlet center

4 Conclusions

In summary, a three-dimensional numerical simulation method was used to investigate the thermal effects of bifurcation stenosis on blood flow and temperature responses. We have investigated the blood velocity and pressure distribution and wall shear stress in arterial bifurcation and its effects on the heat transfer. The results indicated that the maximum wall shear stress was located on stenosis. The pressure distribution of two branch vessels was effectively remodeled by stenosis. In addition, heat transfer between blood with solid tissue was also affected by bifurcation stenosis due to the inhomogeneous distribution of blood velocity. This work may enhance the current understanding of the factors for determining the effects of bifurcation stenosis in the vascular network [24,25].

Acknowledgement: We would also like to thank the editors for many helpful suggestions.

Funding Statement: This work is supported by the National Natural Science Foundation of China (NSFC) under Grant No. 52076213.

Conflicts of Interest: The authors declare that there is no conflict of interest.

References

1. Wang, H. D., Naghavi, M., Allen, C., Barber, R. M., Bhutta, Z. A. et al. (2016). Global, regional, and national life expectancy, all-cause mortality, and cause-specific mortality for 249 causes of death, 1980–2015: A systematic analysis for the Global Burden of Disease Study 2015. *Lancet*, 388(10053), 1459–1544. DOI 10.1016/S0140-6736(16)31012-1.
2. Asakura, T., Karino, T. (1990). Flow patterns and spatial-distribution of atherosclerotic lesions in human coronary arteries. *Circulation Research*, 66(4), 1045–1066. DOI 10.1161/01.RES.66.4.1045.
3. Cebal, J. R., Vazquez, M., Sforza, D. M., Houzeaux, G., Tateshima, S. et al. (2015). Analysis of hemodynamics and wall mechanics at sites of cerebral aneurysm rupture. *Journal of NeuroInterventional Surgery*, 7(7), 530–536. DOI 10.1136/neurintsurg-2014-011247.
4. Zhang, C., Xie, S., Li, S. Y., Pu, F., Deng, X. Y. et al. (2012). Flow patterns and wall shear stress distribution in human internal carotid arteries: The geometric effect on the risk for stenoses. *Journal of Biomechanics*, 45(1), 83–89. DOI 10.1016/j.jbiomech.2011.10.001.
5. Cheruvu, C., Naoum, C., Blanke, P., Norgaard, B., Leipsic, J. (2016). Beyond stenosis with fractional flow reserve via computed tomography and advanced plaque analyses for the diagnosis of lesion-specific ischemia. *Canadian Journal of Cardiology*, 32(11), 1315.e1–1315.e9. DOI 10.1016/j.cjca.2016.01.023.
6. Koskinas, K. C., Feldman, C. L., Chatzizisis, Y. S., Coskun, A. U., Jonas, M. et al. (2010). Natural history of experimental coronary atherosclerosis and vascular remodeling in relation to endothelial shear stress. *Circulation*, 121(19), 2092–2101. DOI 10.1161/CIRCULATIONAHA.109.901678.
7. Hoef, T., Meuwissen, M., Piek, J. J. (2013). Fractional flow reserve and beyond. *Heart*, 99(22), 1699–1705. DOI 10.1136/heartjnl-2012-302325.
8. Chiastra, C., Gallo, D., Tasso, P., Iannaccone, F., Migliavacca, F. et al. (2017). Healthy and diseased coronary bifurcation geometries influence near-wall and intravascular flow: A computational exploration of the hemodynamic risk. *Journal of Biomechanics*, 58, 79–88. DOI 10.1016/j.jbiomech.2017.04.016.
9. Zhang, D. F., Lv, S. Z., Song, X. T., Yuan, F., Xu, F. et al. (2015). Fractional flow reserve versus angiography for guiding percutaneous coronary intervention: A meta-analysis. *Heart*, 101(6), 455–462. DOI 10.1136/heartjnl-2014-306578.
10. Gholipour, A., Ghayesh, M. H., Zander, A. (2018). Nonlinear biomechanics of bifurcated atherosclerotic coronary arteries. *International Journal of Engineering Science*, 133, 60–83. DOI 10.1016/j.ijengsci.2018.08.003.
11. Chiastra, C., Iannaccone, F., Grundeken, M. J., Gijssen, F. J. H., Segers, P. et al. (2016). Coronary fractional flow reserve measurements of a stenosed side branch: a computational study investigating the influence of the bifurcation angle. *BioMedical Engineering OnLine*, 15(1), 1699. DOI 10.1186/s12938-016-0211-0.

12. Cutri, E., Zunino, P., Morlacchi, S., Chiastra, C., Migliavacca, F. (2013). Drug delivery patterns for different stenting techniques in coronary bifurcations: A comparative computational study. *Biomechanics and Modelling in Mechanobiology*, 12(4), 657–669. DOI 10.1007/s10237-012-0432-5.
13. Otero-Cacho, A., Aymerich, M., Flores-Arias, M. T., Abal, M., Alvarez, E. et al. (2018). Determination of hemodynamic risk for vascular disease in planar artery bifurcations. *Scientific Reports*, 8(1), 1459. DOI 10.1038/s41598-018-21126-1.
14. Hossain, S. M. C., Zhang, X., Liu, Z. F., Haider, Z., Memon, K. et al. (2018). Evaluation effect of magnetic field on nanofluid flow through a deformable bifurcated arterial network. *International Communications in Heat and Mass Transfer*, 98(1), 239–247. DOI 10.1016/j.icheatmasstransfer.2018.09.004.
15. Chakravarty, S. S., Mandal, P. K. (2009). Effect of heat and mass transfer on non-Newtonian flow-Links to atherosclerosis. *International Journal of Heat and Mass Transfer*, 52(25–26), 5719–5730. DOI 10.1016/j.ijheatmasstransfer.2009.04.040.
16. Wang, Z., Zhao, G., Wang, T., Yu, Q. F., Su, M. Y. et al. (2015). Three-dimensional numerical simulation of the effects of fractal vascular trees on tissue temperature and intracellular ice formation during combined cancer therapy of cryosurgery and hyperthermia. *Applied Thermal Engineering*, 90(1), 296–304. DOI 10.1016/j.applthermaleng.2015.06.103.
17. Zheng, Y. C., Wu, J. H., He, Z. Z., Huang, S. J. (2018). Computational study of the effects of arterial bifurcation on the temperature distribution during cryosurgery. *BioMedical Engineering OnLine*, 17(1), 157. DOI 10.1186/s12938-018-0438-z.
18. Zhang, Y., Xie, H. W. (2018). The effect of a bifurcation structure on the heat transfer and temperature distribution of pulsatile blood flow. *International Journal of Heat and Mass Transfer*, 118(6), 663–670. DOI 10.1016/j.ijheatmasstransfer.2017.11.055.
19. Zakaria, H., Robertson, A. M., Kerber, C. W. (2008). A parametric model for studies of flow in arterial bifurcations. *Annals Biomedical Engineering*, 36(9), 1515–1530. DOI 10.1007/s10439-008-9531-y.
20. Johnson, D. A., Naik, U. P., Beris, A. N. (2011). Efficient implementation of the proper outlet flow conditions in blood flow simulations through asymmetric arterial bifurcations. *International Journal for Numerical Methods in Fluids*, 66(11), 1383–1408. DOI 10.1002/fld.2319.
21. Gijssen, F. J., van de Vosse, F. N., Janssen, J. D. (1999). The influence of the non-Newtonian properties of blood on the flow in large arteries: steady flow in a carotid bifurcation model. *Journal of Biomechanics*, 32(6), 601–608. DOI 10.1016/S0021-9290(99)00015-9.
22. Hossein, R. J., Pakravan, H. A., Saidi, M. S., Firoozabadi, B. (2019). Primary stenosis progression versus secondary stenosis formation in the left coronary bifurcation: A mechanical point of view. *Biocybernetics and Biomedical Engineering*, 39(1), 188–198. DOI 10.1016/j.bbe.2018.11.006.
23. Nagargoje, M., Gupta, R. (2020). Effect of asymmetry on the flow behavior in an idealized arterial bifurcation. *Computer Methods in Biomechanics and Biomedical Engineering*, 23(6), 232–247. DOI 10.1080/10255842.2019.1711068.
24. Tang, Y. L., Mu, L. Z., He, Y. (2020). Numerical simulation of fluid and heat transfer in biological tissue containing the exact structure of microvascular network using immersed boundary method. *Fluid Dynamics & Materials Processing*, 16(2), 281–296. DOI 10.32604/fdmp.2020.06760.
25. Khechiba, A., Benakcha, Y., Ghezal, A., Spetiri, P. (2018). Combined MHD and pulsatile flow on porous medium. *Fluid Dynamics & Materials Processing*, 14, 137–154.